Acta Crystallographica Section B
**Structural Science**
ISSN 0108-7681

# Molecular interactions in crystalline dibromomethane and diiodomethane, and the stabilities of their high-pressure and low-temperature phases

**Marcin Podsiadło,[a] Kamil Dziubek,[a] Marek Szafrański[b] and Andrzej Katrusiak[a]***

[a]Faculty of Chemistry, Adam Mickiewicz University, Grunwaldzka 6, 60-780 Poznań, Poland, and [b]Faculty of Physics, Adam Mickiewicz University, Umultowska 85, 61-614 Poznań, Poland

Correspondence e-mail: katran@amu.edu.pl

Received 24 May 2006
Accepted 30 August 2006

Dibromomethane, $CH_2Br_2$, and diiodomethane, $CH_2I_2$, have been *in situ* pressure-crystallized in a diamond–anvil cell and their structures determined by single-crystal X-ray diffraction at 0.61 and 0.16 GPa, respectively. The pressure-frozen $CH_2Br_2$ crystal is isostructural with its *C*2/*c* phase obtained by cooling. $CH_2I_2$ is known to form several phases at low temperature, one of which is isostructural with $CH_2Br_2$. However, pressure freezing leads to the polar *Fmm*2 phase. The formation of the polar $CH_2I_2$ structure at 0.16 GPa has been rationalized by the electrostatic and anisotropic van der Waals interactions of the I atoms. No ferroelectric behaviour of the *Fmm*2 polar phase II of $CH_2I_2$ has been determined. The diffraction, calorimetric and dielectric constant studies reveal considerable temperature hysteresis of transformations between the $CH_2I_2$ phases, as well as metastable regions strongly dependent on the sample shape and history.

## 1. Introduction

Dihalomethanes constitute an intriguing series of compounds, the crystal structures of which are mainly governed by halogen···halogen, hydrogen···halogen and weak electrostatic interactions between the polar molecules. Since the molecules of dihalomethanes are relatively small, rigid and $C_{2v}(mm)$-symmetric, they are convenient model compounds for studying intermolecular interactions and their structural implications. In the crystal structures of previously studied halogenated ethanes, molecular disorder was observed (Bujak *et al.*, 2004; Bujak & Katrusiak, 2004). The intermolecular forces involving halogen atoms can be considerably modified by elevated pressure. Such studies have been successfully conducted in various classes of biologically active materials (*e.g.* Boldyreva *et al.*, 2004). The present study of pressure-frozen $CH_2Br_2$ and $CH_2I_2$ was aimed at establishing the high-pressure structures of these compounds, and comparing them with the low-pressure phases and previously investigated dichloromethane (Podsiadło *et al.*, 2005). The physical and chemical properties of solid dibromo- and diiodomethane have been studied using Raman and IR spectroscopy (Anderson *et al.*, 1987; Brown *et al.*, 1969; Lee & Anderson, 1996; Marzocchi *et al.*, 1966; Shimizu, 1985; Torrie *et al.*, 1987; Zhou *et al.*, 1996) and their crystal structures determined at low temperature (Kawaguchi *et al.*, 1973; Prystupa *et al.*, 1989). While the crystals of $CH_2Cl_2$ and $CH_2Br_2$ are believed to be monomorphic at ambient pressure, several phases of $CH_2I_2$ have been observed. At 279 K, $CH_2I_2$ crystallizes in the space group *C*2/*c* (isostructural with the crystal of $CH_2Br_2$) and below 278.5 K this *C*2/*c* phase of $CH_2I_2$ (phase I) becomes metastable, and after minutes or hours (depending on

temperature and size of the sample) the crystal transforms to the *Fmm*2 phase II (Stone, 1932; Torrie *et al.*, 1987). It was observed that transformations of $CH_2I_2$ strongly depend on the cooling rate of the sample: when cooled slowly, the *Fmm*2 phase II persists until 16 K, while quick cooling of phase I generates the *C*2/*c* metastable phase I′ which in turn near 50 K transforms reversibly to phase III, which is isostructural with phases I and I′ according to Prystupa *et al.* (1989). Phases I′ and III coexist with the *Fmm*2 phase II (Prystupa *et al.*, 1989). When left at 258 K, phase I transforms into phase II after *ca* 30 min (Torrie *et al.*, 1987). On warming, phase I′ transforms to phase II near 200 K.

In the series of homologous dichloro-, dibromo- and diiodomethane only phase II of $CH_2I_2$ is polar, while the other structures are centrosymmetric. These noncentrosymmetric and polar symmetry properties are required for applications of crystals as opto-electronic transducers, second-harmonic generators, ferroelectric memories *etc.* Meanwhile, the factors responsible for the centro- or noncentrosymmetric molecular arrangements in crystals are not fully understood. The polar arrangement of $CH_2I_2$ molecules in phase II prompted us to investigate its dielectric properties, seeking possible ferroelectric transformations. We have also reinvestigated the thermal behaviour of $CH_2I_2$ described in the literature (Torrie *et al.*, 1987; Prystupa *et al.*, 1989), in order to provide new information on the transformations between the *C*2/*c* and *Fmm*2 phases, and have carried out temperature-dependent X-ray diffraction experiments. Although similar investigations have already been reported (Prystupa *et al.*, 1989), the region of temperature close to the melting point has not been examined thoroughly. The occurrence of two forms in the freezing region, and their small freezing-point difference of 0.5 K were carefully investigated by Stone (1932). Kawaguchi *et al.* (1973) reported the structure of the monoclinic phase I at 253 K, while according to Torrie *et al.* (1987) and to Prystupa *et al.* (1989) this temperature is close to the phase transition, but on the side of phase II. It was confirmed that the cooling rate is a crucial factor for the transition temperatures (Torrie *et al.*, 1987; Marzocchi *et al.*, 1966) and coexistence of the phases (Prystupa *et al.*, 1989). Apart from diffractometric experiments, we have employed dielectric and calorimetric methods to monitor the regions of stability and transformations of $CH_2I_2$ phases, as well as changes of molecular dynamics in the crystalline state.

## 2. Experimental

Dibromomethane (m.p. 221 K), analytical grade from Polskie Odczynniki Chemiczne, and diiodomethane (m.p. 279 K), 99% purity from Sigma-Aldrich, were used without further purification. The single crystals of these compounds were crystallized *in situ* in a four-pin diamond–anvil cell (DAC). Gaskets made of 0.2 mm inconel and 0.1 mm carbon–steel foils were used for $CH_2Br_2$ and $CH_2I_2$, respectively. The holes in the gaskets were spark-eroded: for the $CH_2Br_2$ measurement after the indentation, the hole was 0.10 mm in height and 0.47 mm in diameter; for $CH_2I_2$, the hole was 0.09 mm in height and 0.43 mm in diameter (these were the dimensions of the pressure-frozen crystals). At 295 K the compounds froze as a polycrystalline mass filling the whole high-pressure chamber volume, at *ca* 0.61 and 0.16 GPa, respectively, calibrated by the ruby-fluorescence method (Barnett *et al.*, 1973; Piermarini *et al.*, 1975) using a BETSA PRL spectrometer with an accuracy of 50 MPa. The polycrystals of $CH_2Br_2$ and $CH_2I_2$ were heated using a hot-air gun, to *ca* 373 and 443 K, respectively, until all but one crystallite melted. Then the DAC was slowly cooled to room temperature, where in each case the single crystal filled the whole volume of the chamber. The freezing of $CH_2Br_2$ and $CH_2I_2$ is illustrated in Figs. 1 and 2, respectively.

Interestingly, the single crystal of $CH_2I_2$ initially grew in the form of a needle (Fig. 2*a*), and then at *ca* 435 K the needle started to grow thicker and became a plate covering half of the high-pressure chamber (Fig. 2*b*). Only when the crystal had no space to expand in the direction perpendicular to the diamond culets did the crystallization progress towards the other half of the chamber to eventually fill it entirely at 295 K (Fig. 2*c*).

The single-crystal reflection data for both dihalomethanes were collected using a KM-4 CCD diffractometer with graphite-monochromated Mo $K\alpha$ radiation at 295 K. The centring of the DAC was performed using the gasket-shadow method (Budzianowski & Katrusiak, 2004). The reflections were collected using the $\omega$-scan technique, 0.9° frame widths and 40 s exposures for $CH_2Br_2$, and 0.85° $\omega$-frames and 40 s exposures for $CH_2I_2$ (Budzianowski & Katrusiak, 2004). For data collections, determination of the *UB* matrices (Busing & Levy, 1967), initial data reductions and *Lp* corrections the *CrysAlis* program suite was used (Oxford Diffraction, 2004). The intensities of the reflections have been corrected for the effects of absorption of X-rays by the DAC, shadowing of the beams by the gasket edges and absorption of the sample crystals themselves (Katrusiak, 2003), and the unit-cell dimensions were corrected for the effects of crystal absorption and beam shadowing by the gasket (Katrusiak, 2004). The structures were solved by direct methods using program *SHELXS*97 (Sheldrick, 1997), and refined with anisotropic displacement parameters for non-H atoms (except for the C1 atom from the pressure-frozen $CH_2Br_2$ structure) using the program *SHELXL*97 (Sheldrick, 1997). Selected crystal data and details of the refinements of pressure-frozen $CH_2Br_2$ and $CH_2I_2$ are listed in Table 1.[1] Attempts to refine the C1 atom anisotropically resulted in a very narrow ellipsoid elongated perpendicular to the Br1–C1–Br2 plane. It was interpreted as being caused by strong anisotropic vibrations of C1 about the intramolecular Br1···Br2 axis. Owing to the unrealistic shape of the ellipsoid, the isotropic model has been applied to refine C1 in the final cycles. The observed difference between the C1–Br1 and C1–Br2 lengths of 0.076 (22) Å (Table 2) is slightly larger than 3 e.s.d.'s, but most likely due to the

[1] Supplementary data for this paper are available from the IUCr electronic archives (Reference: BK5037). Services for accessing these data are described at the back of the journal.

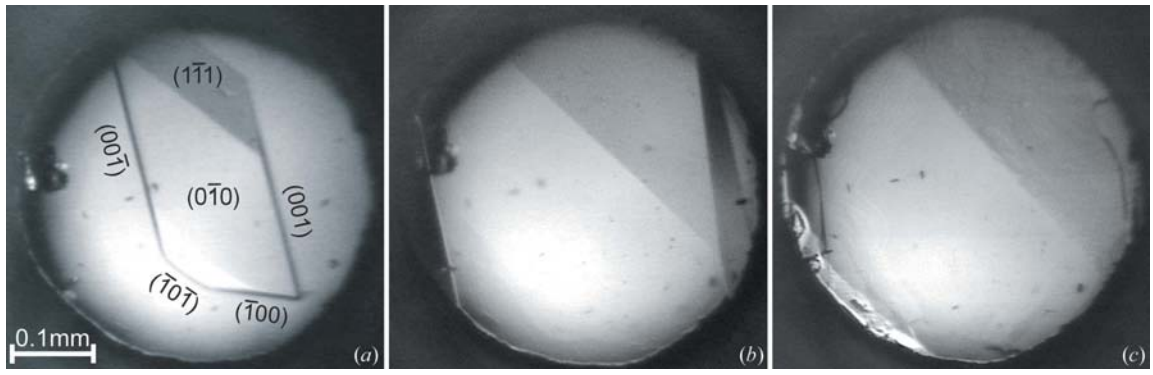


**Figure 1**
Three stages of the $CH_2Br_2$ single-crystal isochoric freezing in the DAC at 0.61 GPa (*c*). The ruby chip for pressure calibration (Barnett *et al.*, 1973; Piermarini *et al.*, 1975) is at the upper-left (at 10 o'clock) edge of the chamber. The crystal faces have been indexed in (*a*).

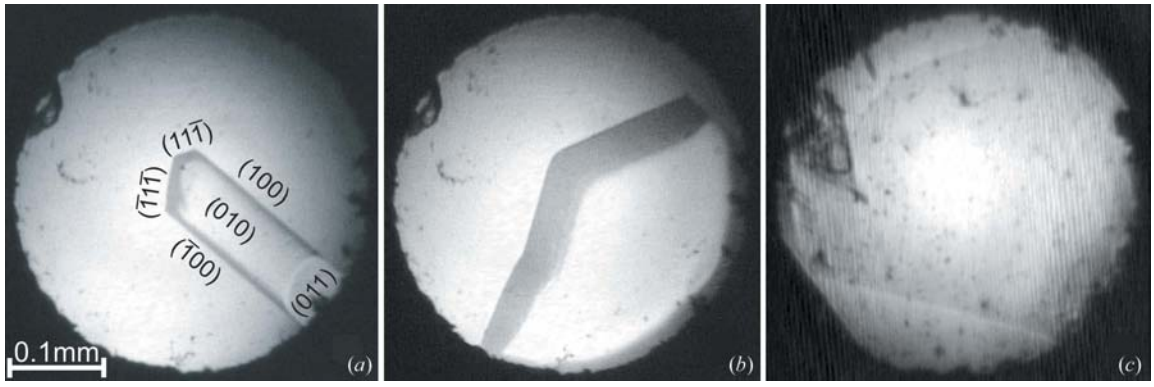


**Figure 2**
The $CH_2I_2$ single-crystal isochoric growth stages in the DAC: the crystal seed at (*a*) 440 K, (*b*) 430 K and (*c*) 295 K and 0.16 GPa. The ruby chip for pressure calibration (Barnett *et al.*, 1973; Piermarini *et al.*, 1975), attached to the upper-left edge of the gasket (*a*, *b*) is pressed against the upper culet by the growing crystal (*c*). The Miller indices of the crystal faces are shown in (*a*).

discrepancies between the harmonic isotropic model and real anharmonic and anisotropic vibrations, additionally aggravated by weak scattering of C compared with Br and low completeness of the high-pressure data.

The $CH_2Br_2$ molecule is located in a general position in the unit cell, while the $CH_2I_2$ molecule occupies a special $C_{2v}(mm)$ site. In the $CH_2Br_2$ model, the H atoms were positioned geometrically with the C–H bond length constrained to 0.97 Å (Sheldrick, 1997) and their isotropic displacement parameters set at $1.2U_{iso}$(C1). In the $CH_2I_2$ model, restraints were applied to obtain a C–H bond length of 1.01 Å and an H–C–H angle of 109.45°. The isotropic displacement parameter of H1 was constrained to $1.3U_{eq}$(C1).

The low-temperature $CH_2I_2$ single-crystal measurements were performed in a 0.3 mm-diameter glass capillary mounted on a KM-4 CCD diffractometer with graphite-monochromated Mo $K\alpha$ radiation. The temperature was controlled using an Oxford Diffraction Cryosystems CPC611 low-temperature attachment. While the liquid sample was cooled at a rate of 1 K min$^{-1}$, its changes were observed through a microscope and by recording 30 s diffraction images. The sample froze at *ca* 220 K giving a diffraction image characteristic of powder. Then the sample was heated at the same rate to *ca* 275 K in order to grow a single crystal suitable for the diffraction experiment. The single-crystal measurement was performed at 270 K. The data were consistent with those of orthorhombic *Fmm*2 phase II (*cf.* Table 1). Then the crystal was cooled to 240 K and a short diffraction measurement was performed, which confirmed the unit-cell parameters and the systematic absences of the space group *Fmm*2. The sample was then heated again and the recorded diffraction images did not show any changes that could be interpreted as a phase transition. The sample finally melted at 278 K, which was observed visually and confirmed by diffraction images typical of liquids.

The differential scanning calorimetric (DSC) measurement was carried out using a Linkam DSC 600 calorimeter at ambient pressure under a nitrogen atmosphere in an aluminium crucible. The DSC signal was recorded in the cooling and heating runs between 297 and 183 K with a temperature-change rate of 2 K min$^{-1}$.

Measurements of electric permittivity were carried out in the frequency range from 1 kHz to 10 MHz with a Hewlett-Packard 4192A impedance analyzer. A plate capacitor filled at room temperature with liquid $CH_2I_2$ was cooled/heated with a temperature rate of 0.1–0.5 K min$^{-1}$. The temperature was measured using a copper–constantan thermocouple in thermal contact with the sample. The amplitude of the AC measuring electric field was 5 V cm$^{-1}$. Tests for the presence of a ferroelectric hysteresis loop were performed using the Diamant–Drenck–Pepinsky bridge method at a frequency of 50 kHz.

**Table 1**
Crystal data and details of the refinements of $CH_2Br_2$ at 0.61 GPa/295 K, $CH_2I_2$ at 0.16 GPa/295 K, and $CH_2I_2$ at 0.10 MPa/270 K.

| | $CH_2Br_2$ at 0.61 (5) GPa | $CH_2I_2$ at 0.16 (5) GPa | $CH_2I_2$ at 0.10 MPa |
|---|---|---|---|
| Crystal data | | | |
| Chemical formula | $CH_2Br_2$ | $CH_2I_2$ | $CH_2I_2$ |
| $M_r$ | 173.85 | 267.83 | 267.83 |
| Cell setting, space group | Monoclinic, *C*2/*c* | Orthorhombic, *Fmm*2 | Orthorhombic, *Fmm*2 |
| Temperature (K) | 295 (2) | 295 (2) | 270.0 (5) |
| *a*, *b*, *c* (Å) | 12.031 (2), 4.3385 (9), 14.795 (3) | 7.3128 (15), 13.074 (3), 4.7465 (9) | 7.411 (3), 13.137 (4), 4.7942 (15) |
| $\beta$ (°) | 109.51 (3) | 90.00 | 90.00 |
| $V$ (Å$^3$) | 727.9 (3) | 453.82 (16) | 466.8 (3) |
| $Z$ | 8 | 4 | 4 |
| $D_x$ (Mg m$^{-3}$) | 3.173 | 3.920 | 3.812 |
| Radiation type | Mo $K\alpha$ | Mo $K\alpha$ | Mo $K\alpha$ |
| $\mu$ (mm$^{-1}$) | 22.00 | 13.64 | 13.26 |
| Crystal form, colour | Cylinder, colourless | Cylinder, colourless | Cylinder, colourless |
| Crystal size (mm) | 0.47 × 0.47 × 0.10 | 0.43 × 0.43 × 0.09 | 0.12 × 0.12 × 0.12 |
| Data collection | | | |
| Diffractometer | Kuma KM4CCD $\kappa$ geometry | Kuma KM4CCD $\kappa$ geometry | Kuma KM4CCD $\kappa$ geometry |
| Data collection method | $\omega$ scans | $\omega$ scans | $\omega$ scans |
| Absorption correction | Analytical | Analytical | None |
| $T_{min}$ | 0.03 | 0.11 | – |
| $T_{max}$ | 0.09 | 0.26 | – |
| No. of measured, independent and observed reflections | 2222, 330, 170 | 1030, 170, 162 | 530, 298, 265 |
| Criterion for observed reflections | $I > 4\sigma(I)$ | $I > 4\sigma(I)$ | $I > 4\sigma(I)$ |
| $R_{int}$ | 0.178 | 0.075 | 0.148 |
| $\theta_{max}$ (°) | 30.1 | 29.2 | 29.1 |
| Refinement | | | |
| Refinement on | $F^2$ | $F^2$ | $F^2$ |
| $R[F^2 > 2\sigma(F^2)]$, $wR(F^2)$, $S$ | 0.068, 0.149, 0.89 | 0.026, 0.076, 1.33 | 0.063, 0.177, 1.14 |
| No. of parameters | 25 | 14 | 14 |
| H-atom treatment | Constrained to parent site | Mixture of independent and constrained refinement | Mixture of independent and constrained refinement |
| Weighting scheme | $w = 1/[\sigma^2(F_o^2) + (0.065P)^2]$, where $P = (F_o^2 + 2F_c^2)/3$ | $w = 1/[\sigma^2(F_o^2) + 16.8177P]$, where $P = (F_o^2 + 2F_c^2)/3$ | $w = 1/[\sigma^2(F_o^2) + (0.1205P)^2 + 2.0615P]$, where $P = (F_o^2 + 2F_c^2)/3$ |
| $(\Delta/\sigma)_{max}$ | <0.0001 | 0.015 | 0.006 |
| $\Delta\rho_{max}$, $\Delta\rho_{min}$ (e Å$^{-3}$) | 0.57, −0.57 | 0.44, −0.54 | 1.72, −2.10 |
| Extinction method | *SHELXL* | *SHELXL* | *SHELXL* |
| Extinction coefficient | 0.0017 (9) | 0.0123 (14) | 0.015 (3) |
| Absolute structure | – | Flack (1983) | Flack (1983) |
| Flack parameter | – | 0.2 (7) | 0.6 (10) |

Computer programs used: *CrysAlis* (Oxford Diffraction, 2004), *SHELXS*97, *SHELXL*97 (Sheldrick, 1997), *XP* (Siemens, 1990).

The *GAUSSIAN*03 program suite and a PC were used for calculating the electrostatic potential on the molecular surface of diiodomethane (Frisch *et al.*, 2003). The DFT calculations were carried out at the B3LYP/3-21G** level of theory. The electrostatic potential was mapped onto the molecular surface defined as a 0.001 a.u. electron-density envelope (Bader *et al.*, 1987).

## 3. Discussion

### 3.1. Pressure-frozen $CH_2Br_2$ structure

The freezing pressure of $CH_2Br_2$ was determined by the *in situ* crystallization in the DAC at 0.61 (5) GPa/295 K, when the compound froze as a polycrystal filling the whole volume of the high-pressure chamber. This freezing pressure of $CH_2Br_2$ agrees well with the value of 0.65 GPa at 300 K previously determined by Shimizu (1985) by Raman and FT-IR measurements. The $CH_2Br_2$ molecules lie in general positions, but they are almost exactly parallel to crystallographic planes (001) at $z$ = 1/8, 3/8 *etc*. In the pressure-frozen structure the inclination of the molecular plane, defined by atoms Br1—C—Br2 ($\omega$ angle), to the (001) plane is 1.46 (13)°. At 183 K/0.1 MPa this molecular inclination, of 11.59°, is significantly larger (Kawaguchi *et al.*, 1973), and thus the planar arrangement of molecules is less apparent (see Fig. 3). The specific orientation of the $C_{2v}$ symmetric $CH_2Br_2$ molecules can be regarded as a local (referring only to the molecular position and not to its surrounding) pseudosymmetry of a mirror plane parallel to (001) and a twofold axis almost parallel to [010] and passing through the C1 atom. Inter- and intramolecular distances and angles in the low-temperature and high-pressure $CH_2Br_2$ structures are compared in Table 2. The high-pressure structure of dibromomethane, like the pressure-frozen structure of dichloromethane, can be considered as being built of layers running along the shortest intermolecular Br···Br contacts. Such shortest Br···Br contacts involve the molecules lying on the local pseudo-mirror planes (Fig. 3, Table 2). All

**Table 2**
Selected bond lengths (Å), angles (°) and intermolecular contacts (Å) in the pressure-frozen and low-temperature structures of $CH_2Br_2$.

Angle $\omega$ is the inclination of the molecular Br1—C—Br2 plane to the crystallographic plane (001).

| | 183 K/0.1 MPa† | 15 K/0.1 MPa‡ | 295 K/0.61 GPa§ |
|---|---|---|---|
| Molecular dimensions | | | |
| C—H1 | 1.070 | 1.051 (7) | 0.97 |
| C—H2 | 1.071 | 1.077 (7) | 0.97 |
| C—Br1 | 1.922 | 1.928 (5) | 1.888 (15) |
| C—Br2 | 1.901 | 1.954 (5) | 1.961 (16) |
| Br1···Br2 | 3.165 | 3.188 (4) | 3.201 (3) |
| ∠Br1—C—Br2 | 112 | 110.4 (2) | 112.5 (7) |
| ∠H1—C—H2 | 109.5 | 116.9 (6) | 107.84 |
| Intermolecular contacts | | | |
| Br1···Br2$^{i}$ | 3.623 | 3.551 | 3.490 (3) |
| Br1···Br2$^{ii}$ | 3.788 | 3.621 | 3.623 (3) |
| Br2···Br2$^{iii}$ | 3.801 | 3.784 | 3.868 (12) |
| H2···Br1$^{iv}$ | 3.032 | 3.066 | 3.036 |
| ∠$\omega$ (°) | 11.59 | 13.33 | 1.46 (13) |

† Low-accuracy data according to Kawaguchi *et al.* (1973). ‡ Low-temperature structure of $CD_2Br_2$ by neutron powder diffraction according to Prystupa *et al.* (1989). § This work. Symmetry codes: (i) $-\frac{1}{2}+x, \frac{1}{2}+y, z$; (ii) $-\frac{1}{2}+x, -\frac{1}{2}+y, z$; (iii) $\frac{1}{2}-x, \frac{3}{2}-y, -z$; (iv) $\frac{1}{2}-x, -\frac{1}{2}+y, \frac{1}{2}-z$.

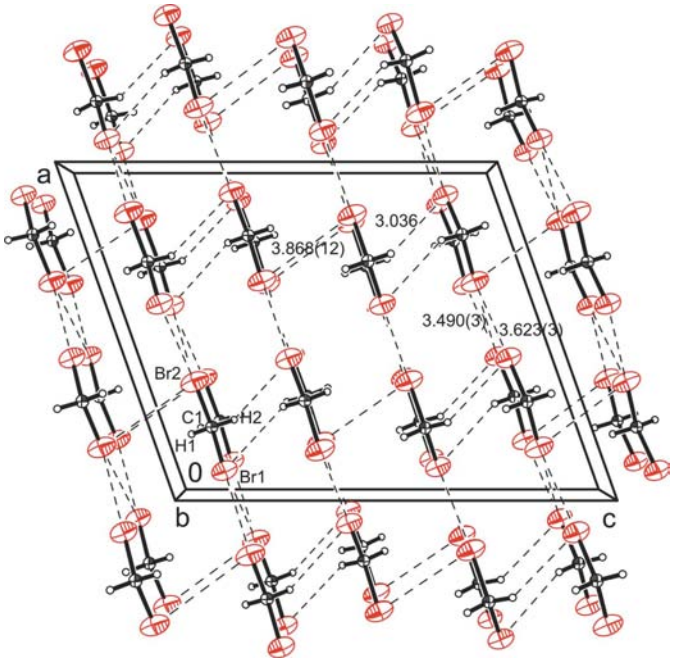


**Figure 3**
The shortest halogen···halogen and H···halogen intermolecular interactions (Å) in the structure of $CH_2Br_2$ projected down [010], indicated by thin dashed lines (*cf.* Table 2). The displacement ellipsoids are shown at the 50% probability level. The non-crystallographic pseudo-mirror plane is parallel to the crystallographic (001) plane.

$CH_2Br_2$ molecules of one layer have the same orientation along [010], and these layers are arranged in pairs in this way, such that in two layers (at $z$ = 1/8 and 3/8 in Fig. 3) the Br atoms of all molecules are oriented along [010], and in the next two layers (at $z$ = 5/8 and 7/8) the Br atoms point at [0$\bar{1}$0]. The shortest of the intermolecular contacts, Br1···Br2$^{i}$ (see Table 2), at 295 K/0.61 GPa is compressed by 0.133 and 0.061 Å relative to the 0.1 MPa structures at 183 K (Kawaguchi *et al.*, 1973) and at 15 K for $CD_2Br_2$ (Prystupa *et al.*, 1989), respectively. The second shortest Br···Br interactions, commensurate with the sum of van der Waals radii (Batsanov, 2001), link the molecules into chains along the crystal direction [100]. This contact is compressed by 0.165 Å between 183 K/0.1 MPa and 295 K/0.61 GPa, while in the high-pressure and 15 K/0.1 MPa structure this distance is practically identical. Surprisingly, the next shortest intermolecular distance between the molecules of the neighbouring planar sheets at $z$ = −1/8 and 1/8 and at $z$ = 3/8 and 5/8 in the 295 K/0.61 GPa structure is longer by about 0.07 Å than at 183 K/0.1 MPa and by 0.084 Å than at 15 K/0.1 MPa. Only one H atom of each $CH_2Br_2$ molecule forms a short H···Br contact between neighbouring planar sheets at $z$ = 1/8 and 3/8 and at $z$ = 5/8 and 7/8 (see Fig. 3).

### 3.2. High-pressure structure of diiodomethane

Diiodomethane froze at 0.16 (5) GPa/295 K, forming a polycrystal filling the whole volume of the high-pressure chamber. Shimizu (1985) determined the freezing pressure of diiodomethane by Raman and FT-IR measurements as 0.14 GPa at 300 K, while the Raman studies by Zhou *et al.* (1996) gave 0.33 (10) GPa at 293 K. We have established that at elevated pressure $CH_2I_2$ freezes in the low-temperature *Fmm*2 phase II. During the pressure-induced crystallization, no other forms of the $CH_2I_2$ crystals were observed.

The $CH_2I_2$ molecules lie on the $C_{2v}$-symmetric sites at the nodes of the *F* lattice. A comparison of inter- and intramolecular distances and angles in $CH_2I_2$ structures is presented in Table 3. The unit-cell parameters of this structure, owing to its relative simplicity, can be related to the closest intermolecular I···I and H···I contacts, which are crucial for the molecular packing. When assuming that the molecular size can be approximated by three dimensions, $l_{H-H}$, $l_{I-I}$ and $l_{H-I}$ (see Fig. 4), the unit-cell parameters depend on the intermolecular interactions according to the formulae

$$a = l_{H-H} + \left[4d_2^2 - l_{I-I}^2 - (d_0 - l_{H-I})^2\right]^{1/2},$$

$$b = 2l_{I-I} + \left[4d_1^2 - (d_0 + l_{H-I})^2\right]^{1/2},$$

$$c = l_{H-I} + d_0,$$

where $d_0 = 0.5[4d_3^2 - l_{I-I}^2 - l_{H-H}^2]^{1/2}$, and $d_1$, $d_2$ and $d_3$ (see Fig. 4) are the shortest intermolecular interactions in the $CH_2I_2$ crystal structure. The reverse relations have the form

$$d_1 = 0.5\left[(b - 2l_{I-I})^2 + c^2\right]^{1/2},$$

$$d_2 = 0.5\left[(a - l_{H-H})^2 + (c - 2l_{H-I})^2 + l_{I-I}^2\right]^{1/2},$$

$$d_3 = 0.5\left[4(c - l_{H-I})^2 + l_{I-I}^2 + l_{H-H}^2\right]^{1/2}.$$

Thus, it appears that the main role in the molecular arrangement is played by the cohesion forces between the closest I···I ($d_1$) and H···I ($d_2$ and $d_3$) atoms. Each molecule interacts in

**Table 3**
Selected bond lengths (Å), angles (°) and intermolecular contacts (Å) in the pressure-frozen and low-temperature structures of $CH_2I_2$ (all data for the *Fmm*2 phase II).

| | 16 K/0.1 MPa† | 30 K/0.1 MPa† | 50 K/0.1 MPa† | 255 K/0.1 MPa† | 270 K/0.1 MPa‡ | 295 K/0.16 GPa‡ |
|---|---|---|---|---|---|---|
| Molecular dimensions | | | | | | |
| C—H | 1.130 (11) | 1.109 (4) | 1.105 (10) | 1.131 (13) | 1.01 | 1.01 |
| C—I | 2.146 (7) | 2.141 (3) | 2.159 (7) | 2.144 (7) | 2.131 (1) | 2.129 (1) |
| ∠I—C—I | 113.7 (3) | 112.8 (1) | 113.2 (2) | 114.2 (2) | 112.96 (5) | 113.27 (4) |
| ∠H—C—H | 113.2 (8) | 110.5 (3) | 110.9 (7) | 105.3 (9) | 110.4 (2) | 109.6 (2) |
| I···I | 3.594 (9) | 3.567 (4) | 3.606 (9) | 3.600 (8) | 3.553 (2) | 3.556 (1) |
| Intermolecular contacts | | | | | | |
| I···I$^{i}$ | 3.710 | 3.736 | 3.716 | 3.806 | 3.852 (1) | 3.810 (1) |
| H···I$^{ii}$ | 3.235 | 3.253 | 3.277 | 3.356 | 3.441 (1) | 3.400 (1) |
| H···I$^{iii}$ | 3.535 | 3.502 | 3.525 | 3.551 | 3.618 (1) | 3.578 (1) |

† Neutron diffraction data according to Prystupa *et al.* (1989). ‡ This work. Symmetry codes: (i) $-x, \frac{1}{2}-y, \frac{1}{2}+z$; (ii) $\frac{1}{2}+x, y, -\frac{1}{2}+z$; (iii) $-x, -y, 1+z$.

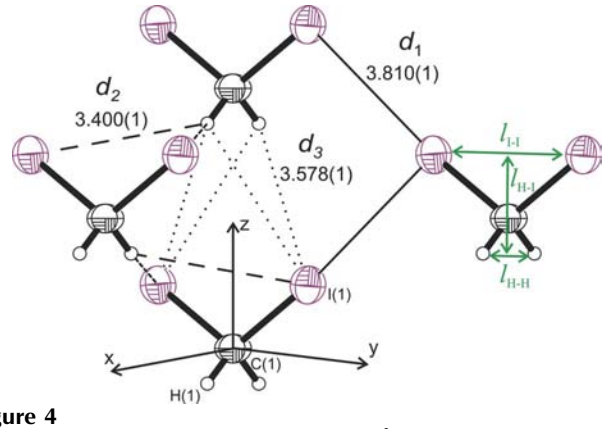


**Figure 4**
The closest contacts of the H and I atoms (Å) in the $CH_2I_2$ structure at 0.16 GPa (distances $d_1$ are indicated by the full lines, $d_2$ by dashed lines and $d_3$ by dotted lines). Thermal ellipsoids are shown at the 50% probability level. Molecular dimensions $l_{H-H}$, $l_{I-I}$ and $l_{H-I}$ are indicated in green.

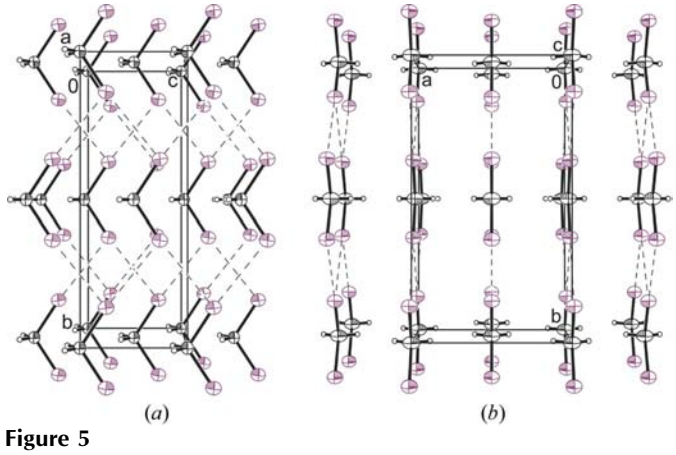


**Figure 5**
Autostereograms (Katrusiak, 2001*a*,*b*) of $CH_2I_2$ at 0.16 GPa/295 K projected along (*a*) [*x*] and (*b*) [*z*] directions. Dashed lines present the shortest I···I intermolecular contacts. Displacement ellipsoids are plotted at the 50% probability level.

this way with its ten neighbours, the vectors between the central and neighbouring molecules being [±0.5 0 ±0.5], [0 ±0.5 ±0.5] and [0 0 ±1]. Distances $d_2$ and $d_3$ are somewhat longer than the sum of the van der Waals radii of the H and I atoms, 3.35 Å according to Batsanov (2001). Each of the H atoms is involved in four such contacts, as shown in Fig. 4: two to the closest molecule down [00$\bar{1}$], and two to the molecule along [10$\bar{1}$].

Phase II of $CH_2I_2$ is polar, whereas the two other dihalomethanes, $CH_2Cl_2$ and $CH_2Br_2$, are centrosymmetric. The polar symmetry of the structure, with the $CH_2I_2$ molecules all oriented in the same direction, may result from the coincidence of molecular dimensions and intermolecular contacts; namely that the $CH_2I_2$ molecules are arranged along planes (100) in this manner, and that the I atoms interact with the H atoms of the neighbouring molecules. In this arrangement the negative net atomic charges of the I atoms are located close to the positive net atomic charges of the H atoms (see Figs. 5 and 6). Such an arrangement could be realised only when the molecular dimension $l_{H-I}$ and the *z* component of the intermolecular distance $d_3$ matched each other in the respect that they optimize the H···I interaction. When assuming isotropic

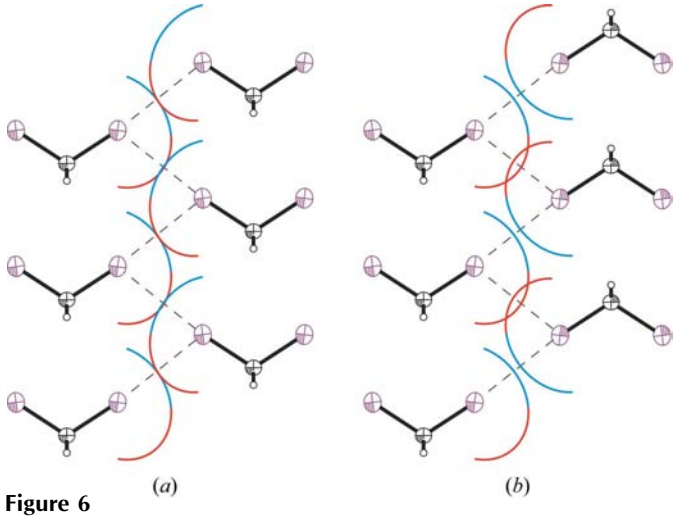


**Figure 6**
One sheet parallel to (100) of interacting $CH_2I_2$ molecules in the *Fmm*2 phase II, with two columns of the molecules along [001] being parallel (*a*). A hypothetical structure with the columns antiparallel, but the iodine atomic positions retained, is presented in (*b*). The major and minor radii of the I atoms, also corresponding to the negative and positive electrostatic potential on the molecular surface, have been indicated in red and blue, respectively (*cf.* Fig. 7). The molecular and van der Waals dimensions have been represented to scale.

I···I interactions, the arrangement of the sheets of $CH_2I_2$ molecules along (100) (at $x = 0$ and $x = 1/2$) could be either parallel or antiparallel. In fact, the antiparallel arrangement appears more favoured because of the interactions of molecular dipoles. However, when assuming anisotropic van der Waals radii of the I atom (Nyburg & Faerman, 1985), the directions of the molecules within (100) sheets cannot be reversed. It can be observed that the I···I interactions ($d_1$ in Fig. 4) are formed along the C—I bond on one side [the C—I—$I^i$ angle is 174.84 (3)°], and almost perpendicular to the C—I bond on the other [the I···$I^i$—C angle is 108.11 (2)°]. According to Nyburg & Faerman (1985), the minor radius of the I atom is shorter by 0.37 Å than its major radius (1.76 Å along the C—I bond, and 2.13 Å perpendicular). These values agree well with the I···I distances observed in pressure-frozen $CH_2I_2$. However, if the (100) sheets were reversed so that their polarizations along [001] were antiparallel, as illustrated in Fig. 6(*b*), the regions around the I atom with the major radius would face the analogous longer radius of the interacting I atom, and the shorter-radius regions would face each other too (Fig. 6*b*).

Moreover, according to Murray *et al.* (1994) the electrostatic potential plotted onto molecular surfaces of tetrahalomethanes is positive at the end regions (*i.e* on the extension of the C—halogen bond) and negative along the rings perpendicular to the C—halogen bonds. More recently, a similar distribution of electrostatic potential was reported for monohalogenated methanes by Brammer *et al.* (2001). This electrostatic potential distribution has been confirmed by our *ab initio* computations for the $CH_2I_2$ molecule (Fig. 7); however, it can be clearly seen that in the diiodomethane the negative charge on the I-atom circumference is considerably higher in the region between the I atoms than in the regions facing the H atoms. The electrostatic potential calculations also illustrate the polarization of the molecule, with the positive charge located at the H atoms. It is apparent that the electrostatic potential anisotropy is important for the molecular aggregation in the crystalline state. This charge distribution explains the head-to-tail arrangement of the molecules in the columns along [001]. In the hypothetical $CH_2I_2$ structure with antiparallel columns of molecules, two types of I···I contacts would be formed: shorter ones along the C—I bonds, and longer ones approximately perpendicular to the C—I bonds. However, such an arrangement, analogous to that shown in Fig. 6(*b*), would require that the lone electron pairs of the I atoms (*i.e.* their negatively charged parts) directed perpendicular to the C—I bonds, be located closely in the crystal structure, and that the positively charged parts of the I-atom surface directed along the C—I bonds be located closely too (*cf.* Fig. 7). Thus, such an arrangement appears to be unfavourable as far as the electrostatic interactions are concerned.

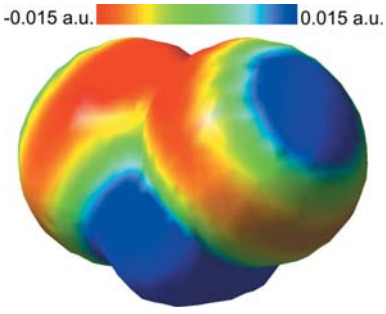


**Figure 7**
The molecular surface of $CH_2I_2$ with its electrostatic potential indicated in the colour scale. The colour scale range spans from −0.015 to 0.015 a.u.

### 3.3. The dielectric permittivity measurement

Temperature dependencies of the real part $\varepsilon'$ of the complex electric permittivity $\varepsilon = \varepsilon' - i\varepsilon''$, measured for $CH_2I_2$ at different rates of temperature change, are plotted in Fig. 8. As $\varepsilon'$ weakly depends on frequency for this compound, the frequency dispersion is negligible and therefore we present only the representative data measured at 10 kHz. There are evident differences between the cooling and heating runs. Also a strong influence of the rate of temperature variation on the dielectric response is observed. When cooling $CH_2I_2$ with a moderate rate of 0.5 K $min^{-1}$ (Fig. 8*a*), a small anomalous increase in $\varepsilon'$ with the onset at $T_{1c} = 286$ K is observed. Further cooling results in a progressive increase in the dielectric constant up to $T_f = 264$ K, at which a sharp first-order phase transition takes place. A sudden drop in the dielectric constant undoubtedly results from the freezing of the electric dipoles in the low-temperature phase. This dielectric response of $CH_2I_2$ is analogous to that of polar liquids, which first freeze into a plastic crystalline phase characterized by a high degree of the orientational freedom of molecular dipoles, and at still lower temperatures undergo a phase transition to a rigid phase. The temperature behaviour of the dielectric constant suggests that in the low-temperature phase the arrangement of the molecular dipoles is antiparallel, which is consistent with the *C*2/*c* phase I of $CH_2I_2$. The parallel (ferroelectric) arrangement is much less likely, which is also consistent with the absence of a ferroelectric hysteresis loop below $T_f = 264$ K and with the $\varepsilon'$ behaviour when the sample was heated.

In the heating run the substance undergoes a different sequence of phase transitions. Just before the reverse transition producing a strong $\varepsilon'$ jump, the crystal enters another phase, which exists in a narrow temperature range. It can be interpreted as the phase transition from the metastable *C*2/*c* phase I, which was obtained by cooling the sample and existed in the whole low-temperature region, to the stable *Fmm*2 phase II. This transition, observed in Fig. 8(*a*) at $T_2 = 278$ K, is clearly discontinuous, similar to the transformations to phase I at $T_f$, and melting of phase II at $T_m$.

In another run the sample was cooled through $T_f$ at a rate of 0.2 K $min^{-1}$ and held at $T = 259$ K for 2 h (see Fig. 8*b*). The reduced rate of cooling from 0.5 to 0.2 K $min^{-1}$ resulted in a large increase in $T_f$, by *ca* 6 K. On further cooling in the solid-state phase the $\varepsilon'$ value started to rise, indicating a rearrangement of molecular dipoles, and this process saturated a few degrees below $T_f$. This behaviour could be interpreted by assuming that just below the freezing point the sample

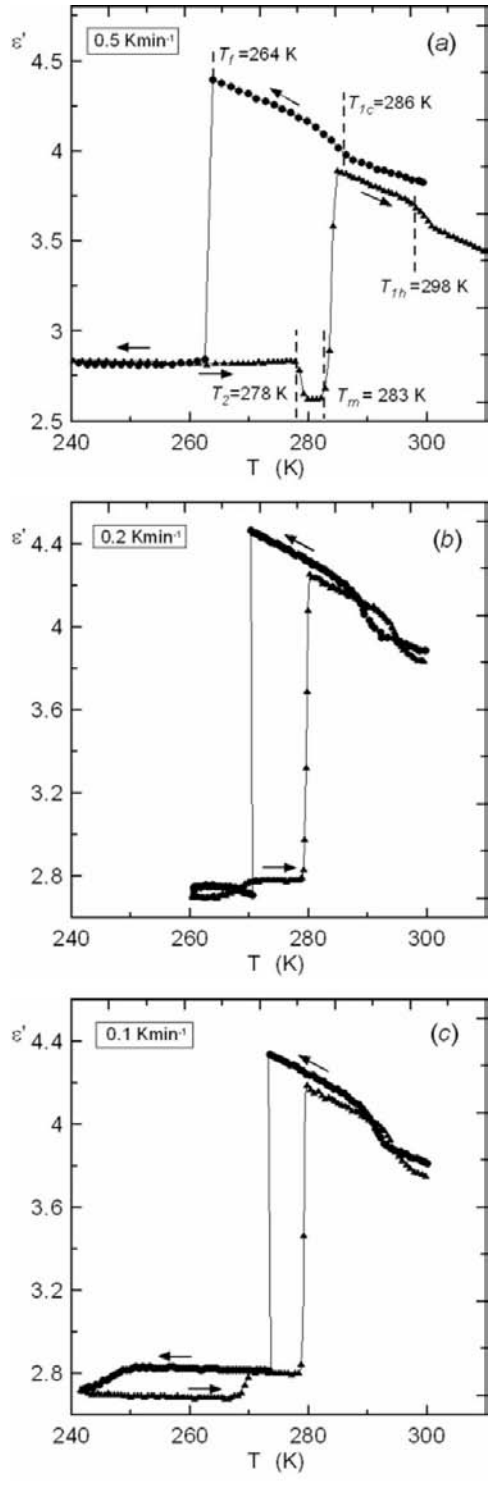


**Figure 8**
Temperature dependencies of the dielectric constant measured for $CH_2I_2$ at 10 kHz in the cooling and heating cycles, as indicated by the arrows. The data were measured at different rates of temperature changes: (*a*) 0.5, (*b*) 0.2 and (*c*) 0.1 K min$^{-1}$. The vertical dashed lines mark the transition temperatures.

consisted of two phases, and during the slow cooling the *C*2/*c* phase I was grown. The dielectric constant of the sample kept at 259 K began to drop, as seen in Fig. 8(*b*), consistent with observations reported by Torrie *et al.* (1987) that the *C*2/*c* phase I transforms into the *Fmm*2 phase II after 30 min at 258 K. Besides, further changes in $\varepsilon'$ indicating a reverse transition were observed between 265 and 270 K on heating the sample. The measurements performed at a rate of 0.1 K min$^{-1}$ are shown in Fig. 8(*c*). At these very slow temperature changes the freezing temperature was increased to $T_f$ = 273.1 K, *i.e.* about 9 K higher than that of the 0.5 K min$^{-1}$ run. The low-temperature part of the plot in Fig. 8(*c*) indicates the presence of two phases with different $\varepsilon'$ values. The transition between these phases occurs with a large temperature hysteresis of about 20 K.

All these dielectric measurements point out the importance of the thermal treatment and history of the sample, which is a consequence of its metastable properties.

### 3.4. Differential scanning calorimetry

The calorimetric study of $CH_2I_2$ fully confirmed the freezing and solid-state transitions observed by dielectric constant measurements discussed above. The recorded DSC runs are shown in Fig. 9. The overcooling of the sample and the absence of changes above *ca* 243 K is a similar effect to that observed in the low-temperature diffraction studies. At 243 K the sample froze in the *C*2/*c* phase I and no other anomaly appeared to 183 K. The freezing temperature is significantly larger, by *ca* 30 K, than that observed in the dielectric measurements. This difference is apparently due to the faster rate of cooling of the sample in the DSC runs. In the heating run the small signal at 275 K can be interpreted as the transition from phase I to phase II. The broad signal immediately after, starting at 278 K, corresponds to the sample melting. A small kink in this signal at 284 K may be due either to the gradual transformations of the sample or to the melting process of two coexisting phases (*i.e.* not all samples transformed into phase II at 275 K) and their different melting points (Stone, 1932).

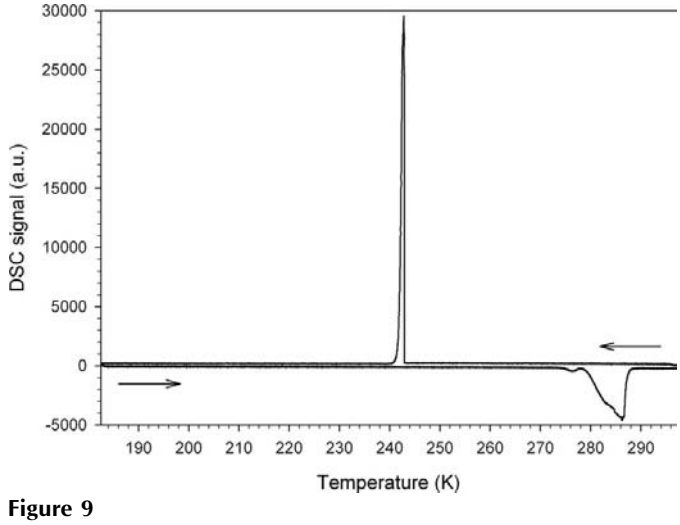


**Figure 9**
Differential scanning calorimetry thermograph for $CH_2I_2$ performed in the 297–183 K range with a rate of 2 K min$^{-1}$. The arrows indicate the direction of the temperature changes.

## 4. Conclusions

Pressure-frozen $CH_2Br_2$ and $CH_2I_2$ crystallize in phases which are stable at low temperature: $CH_2Br_2$ in the *C*2/*c* phase, and $CH_2I_2$ in the *Fmm*2 phase II. It is plausible that the freezing in the stable phase II of $CH_2I_2$ is due to the increased role of tight packing of molecules at elevated pressure. In both these structures the molecular arrangement is governed by halogen···halogen and H···halogen contacts. All phases of $CH_2I_2$ and $CH_2Br_2$ are two-dimensionally isostructural (Fábián & Kálmán, 2004), with the polar sheets clearly illustrating the anisotropic dimensions of the halogen atoms and the electrostatic contribution to their interactions; the crystal structure is additionally stabilized by the attraction between net charges at H and I atoms. Temperature freezing of $CH_2I_2$ leads either to the *C*2/*c* phase I or to the *Fmm*2 phase II, depending on the sample shape, size and history. Different temperature and pressure freezing of $CH_2I_2$ may be due to changes in subtly balanced intermolecular contacts, and to long-range interactions. The detailed analysis of the thermal stability of such a simple model compound as $CH_2I_2$, performed by X-ray diffraction combined with DSC and dielectric measurements, sheds new light on the problem of reproducibility of thermodynamic transformations in the systems where metastable phases occur.

This study was supported by the Polish Ministry of Scientific Research and Information Technology, Grant No. 3T09A18127.

## References


Anderson, A., Torrie, B. H., Danagher, D. J., Laurin, D. G., White, J. K. & Zung, W. W. E. (1987). *J. Raman Spectrosc.* **18**, 97–100.

Bader, R. F. W., Carroll, M. T., Cheeseman, J. R. & Chang, C. (1987). *J. Am. Chem. Soc.* **109**, 7968–7979.

Barnett, J. D., Block, S. & Piermarini, G. J. (1973). *Rev. Sci. Instrum.* **44**, 1–9.

Batsanov, S. S. (2001). *Inorg. Mater.* **37**, 871–885.

Boldyreva, E. V., Drebushchak, T. N., Shakhtshneider, T. P., Sowa, H., Ahsbahs, H., Goryainov, S. V., Ivashevskaya, S. N., Kolesnik, E. N., Drebushchak, V. A. & Burgina, E. B. (2004). *Arkivoc*, **XII**, 128–155.

Brammer, L., Bruton, E. A. & Sherwood, P. (2001). *Cryst. Growth Des.* **1**, 277–290.

Brown, C. W., Obremski, R. J., Allkins, J. R. & Lippincott, E. R. (1969). *J. Chem. Phys.* **51**, 1376–1384.

Budzianowski, A. & Katrusiak, A. (2004). *High-Pressure Crystallography*, edited by A. Katrusiak & P. F. McMillan, pp. 101–112. Dordrecht: Kluwer Academic Publishers.

Bujak, M., Budzianowski, A. & Katrusiak, A. (2004). *Z. Kristallogr.* **219**, 573–579.

Bujak, M. & Katrusiak, A. (2004). *Z. Kristallogr.* **219**, 669–674.

Busing, W. R. & Levy, H. A. (1967). *Acta Cryst.* **22**, 457–464.

Fábián, L. & Kálmán, A. (2004). *Acta Cryst.* B**60**, 547–558.

Flack, H. D. (1983). *Acta Cryst.* A**39**, 876–881.

Frisch, M. J. *et al.* (2003). *GAUSSIAN*03, Revision B.04. Gaussian, Inc., Pittsburgh, PA, USA.

Katrusiak, A. (2001*a*). *J. Mol. Graph. Model.* **19**, 363–367.

Katrusiak, A. (2001*b*). *J. Mol. Graph. Model.* **19**, 398.

Katrusiak, A. (2003). *REDSHABS*. Adam Mickiewicz University, Poznań, Poland.

Katrusiak, A. (2004). *Z. Kristallogr.* **219**, 461–467.

Kawaguchi, T., Wakabayashi, A., Matsumoto, M., Takeuchi, T. & Watanabé, T. (1973). *Bull. Chem. Soc. Jpn*, **46**, 57–61.

Lee, S. A. & Anderson, A. (1996). *Chem. Phys. Lett.* **262**, 337–342.

Marzocchi, M. P., Schettino, V. & Califano, S. (1966). *J. Chem. Phys.* **45**, 1400–1404.

Murray, J. S., Paulsen, K. & Politzer, P. (1994). *Proc. Indian Acad. Sci. (Chem. Sci.)*, **106**, 267–275.

Nyburg, S. C. & Faerman, C. H. (1985). *Acta Cryst.* B**41**, 274–279.

Oxford Diffraction (2004). *Xcalibur CCD system, CrysAlis Software System*, Version 1.171. Oxford Diffraction Ltd, Abingdon, Oxfordshire, UK.

Piermarini, G. J., Block, S., Barnett, J. D. & Forman, R. A. (1975). *J. Appl. Phys.* **46**, 2774–2780.

Podsiadło, M., Dziubek, K. & Katrusiak, A. (2005). *Acta Cryst.* B**61**, 595–600.

Prystupa, D. A., Torrie, B. H., Powell, B. M. & Gerlach, P. N. (1989). *Mol. Phys.* **68**, 835–851.

Sheldrick, G. M. (1997). *SHELXS*97 and *SHELXL*97. University of Göttingen, Germany.

Shimizu, H. (1985). *Solid State Physics Under Pressure*, edited by S. Minomura, pp. 317–322. Terra Scientific Publishing Company.

Siemens (1990). *XP*. Siemens Analytical X-ray Instruments Inc., Madison, Wisconsin, USA.

Stone, H. W. (1932). *J. Am. Chem. Soc.* **54**, 112–114.

Torrie, B. H., Anderson, A., Andrews, B., Laurin, D. G., White, J. K. & Zung, W. W. E. (1987). *J. Raman Spectrosc.* **18**, 215–220.

Zhou, Y., Lee, S. A. & Anderson, A. (1996). *J. Raman Spectrosc.* **27**, 499–502.